Solid-State Electronics 108 (2015) 2–7

Contents lists available at ScienceDirect

Solid-State Electronics

journal homepage: www.elsevier.com/locate/sse

Influence of magnetization variations in the free layer on a non-volatile magnetic flip flop

Thomas Windbacher *, Alexander Makarov, Viktor Sverdlov, Siegfried Selberherr

Institute for Microelectronics, TU Wien, Gußhausstraße 27-29/E360, A-1040 Vienna, Austria

ARTICLE INFO

Article history:
Available online 31 January 2015

The review of this paper was arranged by B. Gunnar Malm

Keywords:
Spintronic
Flip flop
Spin transfer torque
Layer magnetization variations
Thermal field

ABSTRACT

Recently, we proposed an alternative non-volatile magnetic flip flop which allows high integration density. This work extends the up to now gained results to the devices' functionality under statistically distributed magnetization variations of its free layer. Assuming position uncorrelated random fluctuations in the free layer, that the variations are fixed with respect to time, and that small deviations from its mean are more likely than big ones, a Gaussian distribution was chosen to model the random fluctuations. The random variations were added to the simulations as a position dependent Zeeman term and their influence was varied by changing the variance of the distribution scaled in percent of the free layers saturation magnetization. The results with and without thermal excitation show that the flip flop is capable of operating under high free layer field variations.

1. Introduction

Since its very beginnings the semiconductor industry was driven to push the achievable integration density to reduce costs and satisfy the demand for cheap and powerful electronics. This is reflected in the International Technology Roadmap for Semiconductors (ITRS) [1], however, over the years each technology node becomes significantly more expensive and it gets harder to keep control over the CMOS devices. Therefore, in the past new processes, materials, and devices have been introduced several times, e.g., global and local strain techniques, high-k metal gate stacks, 3D FETs. As technology evolved new possible show stoppers like interconnection delay and the devices power consumption appeared [2,3]. This led to the idea to move from normally "ON" circuits and devices to normally "OFF" designs, where latent circuit parts are shut down completely and power will only be consumed, when information is read, written, or processed. The switch from permanently dissipating power systems to only when required spending energy systems demands a reevaluation of all CMOS building blocks. Here, spin as a degree of freedom and its advantageous features like non-volatility, high endurance, and fast operation attract special attention [4]. Besides the self-evident exploitation of spintronics for memory applications, the use of spin also allows to perform logic operations and information transport differently than in state of the art CMOS applications [5,6]. Hence, the paradigm of the Von Neumann architecture and its disadvantages, like the performance limiting information transport between memory and processing units through a common bus, can be eased and may become superfluous in the future. Additionally, merging memory and computation units promises a further boost in integration density.

While spintronic memory applications have become so mature that they start to penetrate the market [7–10], other utilizations are still in the experimental or even conceptual phase [4]. However, not only memory and combinational logic needs a redesign, also sequential logic, e.g. flip flops and latches, requires reconsideration. Even though, there are already non-volatile spintronic flip flops, they are commonly built as CMOS magnetic tunnel junction (MTJ) hybrids [2]. The results are promising with respect to power consumption and speed, but due to the need to convert the signal between the spintronics signal domain (memory) and CMOS domain (computation) every time information is read, written, or processed, additional transistors are necessary which rather decrease the integration density than clears die space [2].

2. Device and operation principle

Therefore, we proposed a non-volatile magnetic flip flop which shifts the actual computation from the CMOS domain to the magnetic domain [11,12]. Thus, one is able to harvest the benefits of spintronics and at the same time denser and simpler layouts are

* Corresponding author.
E-mail addresses: windbacher@iue.tuwien.ac.at (T. Windbacher), makarov@iue.tuwien.ac.at (A. Makarov), sverdlov@iue.tuwien.ac.at (V. Sverdlov), selberherr@iue.tuwien.ac.at (S. Selberherr).

http://dx.doi.org/10.1016/j.sse.2014.12.023
0038-1101/

enabled. The structure comprises three anti-ferromagnetically coupled stacks, two for input *A* and *B* and one for readout *Q*. Each stack features an out-of-plane anisotropy and is connected to the common free layer by a spin barrier (e.g. copper or MgO, see Fig. 1). The common free layer also exhibits an out-of-plane anisotropy and stores the logic information via the magnetic orientation of the free layer. Logic "0" and "1" of the inputs is mapped to the polarity of the input pulses, respectively. A positive current is defined as flowing from one of the inputs towards the free layer (anti-parallel to the *z*-axis), while the electrons flow in the opposite direction (parallel to the *z*-axis).

If now one positive current pulse passes through one of the input stacks (*A* or *B*), the electrons will flow out of the free layer and try to enter the input stack. Since it is easier for electrons with spin parallel to the input stack's orientation to leave the free layer an excess of electrons misaligned to the input stack builds up. They interact with the local free layer's magnetization and excite local precessions. The resulting driving force acts only in the region where the current flows, but through the exchange coupling of the local magnetic moments with their neighbors the precessions start to move out of the polarizer stack overlapping region and travel through the free layer, until they hit the other end, get reflected, move back, get pushed out again and so on [13]. During this kind of oscillating motion, the localized precessions of the magnetic moments in the common free layer are excited and start to build up, until the magnetization eventually passes the energy barrier separating its two stable states and relaxes into the other stable state fast. Applying a second synchronous pulse at the other input stack causes a second spin torque contribution, and the interaction between the two input pulses and their corresponding torques either accelerates (same input polarity) or suppresses (opposing input polarities) the switching of the free layers' magnetization orientation. Therefore, two sufficiently high and long enough pulses with the same polarities either write logic "0" or "1" into the common free layer and two pulses with opposite polarities inhibit each other and the initial magnetization state is held. This behavior perfectly matches the definition of sequential logic whose current output state not only depends on the present inputs but also on former inputs. Inverting one of the inputs even more clearly demonstrates the relation to sequential logic, due to its similarity to RS flip flop logic, but without forbidden input combinations [14].

3. Simulation

The proposed device has been tested for operational functionality and its sensitivity with respect to device size and input current

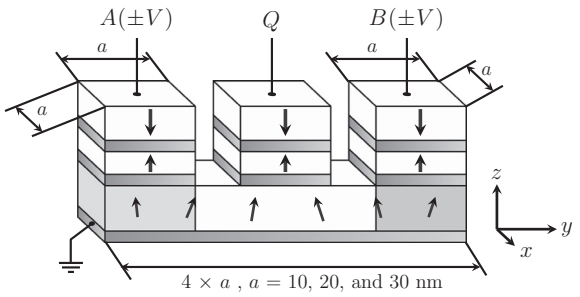

Fig. 1. Proposed non-volatile magnetic flip flop. *A* and *B* denote the inputs for the two spin valve stacks and *Q* denotes the output for the readout stack. The common shared free layer mediates the excited spin precessions. The excited precessions either enforce the switching of the free layer (identical pulse polarities) or quench the switching (opposing pulse polarities). Thus, the flip flop offers SET, RESET, and HOLD operations.

Table 1
Parameters used for simulations.

Parameter	Value
Free layer thickens l	3 nm
Contact sizes a	$(10\,\text{nm})^2, (20\,\text{nm})^2, (30\,\text{nm})^2$
Magnetization saturation M_S	4×10^5 A/m
Out-of-plane uni-axial anisotropy K_1	10^5 J/m^3
Uniform exchange constant A_{exch}	2×10^{-11} J/m
Polarization P	0.3
Spin barrier	*Cu*
Gilbert gyromagnetic ratio γ	2.211×10^5 m/A s
Damping constant α	0.01
Non-adiabatic contribution ϵ'	0.1 [18]
Λ	2
Discretization length $\Delta x, \Delta y$	2 nm
Discretization length Δz	3 nm
Discretization time Δt	1.4875×10^{-14} s
Temperature T	300 K

density variations [11,15]. In order to keep the new results comparable to the previous findings the same parameters and devices have been employed as in [11] (cf. Table 1), but instead of varying the input current density, a Zeeman term has been added to take care of the magnetization variations in the free layer (e.g. variations from grain to grain). The device is modeled with the Landau-Lifshitz-Gilbert equation [16,17]:

$$\frac{\mathrm{d}\vec{m}}{\mathrm{d}t} = \gamma\left(-\vec{m}\times\vec{H}_{\text{eff}} + \alpha\left(\vec{m}\times\frac{\mathrm{d}\vec{m}}{\mathrm{d}t}\right) + \vec{T}\right) \tag{1}$$

$\vec{m}$ denotes the reduced magnetization, $\gamma = 2.211 \times 10^5$ m/As the electron gyromagnetic ratio, $\alpha = 0.01$ the dimensionless damping constant, and $\vec{H}_{\text{eff}}$ the effective field in A/m. The last term in (1) describes the torque acting on the local magnetization due to the polarized electrons. This so called spin transfer torque (STT) $\vec{T}$ is described by the following expression [19]:

$$\vec{T} = \frac{\hbar}{\mu_0 e}\frac{J}{lM_S}\frac{P\Lambda^2}{\left(\Lambda^2+1\right)+\left(\Lambda^2-1\right)\vec{m}\cdot\vec{p}} \cdot\left(\vec{m}\times\vec{p}\times\vec{m} - \epsilon'\vec{m}\times\vec{p}\right) \tag{2}$$

$\hbar$ denotes the Planck constant, μ_0 the permittivity of vacuum, e the electron charge, J the applied current density, l the free layer thickness, M_S the magnetization saturation, P the polarization, $\vec{p}$ the unit polarization direction of the polarized current, and $\Lambda = 2$ a fitting parameter handling non-idealities. Furthermore, $\vec{H}_{\text{eff}}$ is calculated from the functional derivative of the free energy density containing uni-axial anisotropy E_{uni} (10^{-18} J, 4.8×10^{-19} J, and 1.2×10^{-19} J), exchange E_{exch} ($\lessapprox 10^{-23}$ J), and demagnetization contributions (9.3×10^{-19} J, 3.9×10^{-19} J, and 8.5×10^{-20} J at 30 nm, 20 nm, and 10 nm, respectively) [20]. For the sake of completeness also the estimated switching energy as a function of switching time is shown in Fig. 2. The thermal stability factor Δ at 300 K for the 30 nm, 20 nm, and 10 nm layers are ≈ 42, ≈ 25, and ≈ 10, respectively. Furthermore, the devices switching time dependence on width, length, and thickness can be found in [21].

As mentioned before an additional Zeeman term is added to the effective field $\vec{H}_{\text{eff}}$. It is assumed that the variations are uncorrelated with respect to position, randomly distributed throughout the free layer, and fixed in time. It is further contemplated that it is more likely to see small deviations from the out-of-plane magnetization orientation than big differences. Therefore, three Gaussian distributions with random variables ξ_i, mean values of 0 and a variance of 1 for the x, y, and z-axis are presumed (see Fig. 3). The random field $H_{i,\text{rand}}$ is defined as function of the random variables ξ_i,

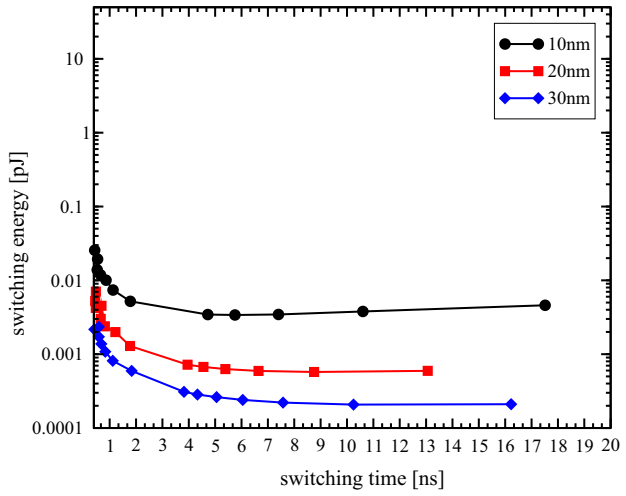

Fig. 2. The energy time delay is estimated as the product of the switching time, the average spin valve resistance (5 Ω) and applied current density times contact area squared.

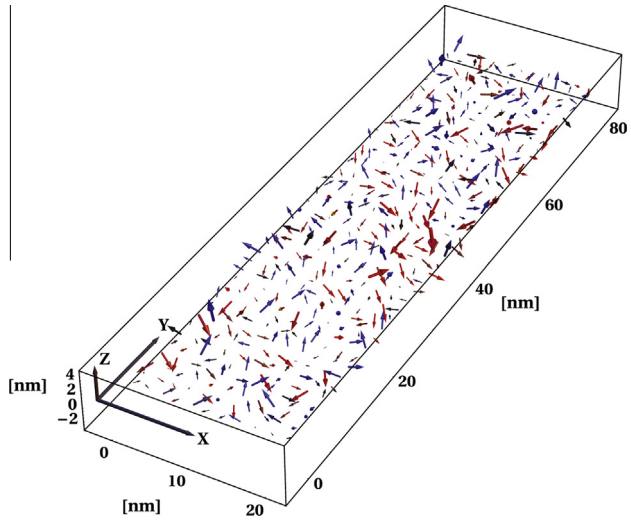

Fig. 3. The added random field is normally distributed. The illustration shows an example for a 20 nm × 80 nm × 3 nm free layer. Blue arrows denote a z-orientation along the z-axis, red arrows describe arrows pointing against the positive z-axis. The arrow thickness and length is proportional to the field strength. (For interpretation of the references to colour in this figure legend, the reader is referred to the web version of this article.)

the free layers magnetization saturation M_S, and the relative strength parameter s:

$$H_{i,\mathrm{rand}} = \xi_i M_S s, \quad i \in \{x,y,z\}. \tag{3}$$

For all three simulated layer sizes from [11] (10 nm × 40 nm × 3 nm, 20 nm × 80 nm × 3 nm, and 30 nm × 120 nm × 3 nm) the parameter s has been set to 0.01, 0.02, 0.05, 0.1, 0.2, 0.5, 0.75, and 1.0, respectively. For each s value 101 random free layer samples have been generated and simulated. The input current density for all simulations was set to a value where all three devices are functional $7. \times 10^{10}$ A/m^2 and take around 10 ns for switching. The pulse window length was chosen 20 ns so the switching events will happen approximately in the middle of the pulse. One input combination for the SET, two for the HOLD operation, and one without any signal for stability checks were calculated.

With a second set of simulations an investigation of the influence of thermal fluctuations has been performed. The temperature influence is modeled by a time dependent Gaussian distributed magnetic field $\vec{H}_{\mathrm{th}}$ [22,23]:

$$H_{i,\mathrm{th}} = \zeta_i \sqrt{\frac{\alpha}{(1+\alpha^2)} \frac{2k_B T}{M_S \gamma \Delta t \, \Delta V}}. \tag{4}$$

Also here, the uncorrelated random variable ζ_i is Gaussian distributed, exhibits $<\zeta_i>=0$, and $<\zeta_i^2>=1$. The temporal realization of the random thermal field $H_{i,\mathrm{th}}$ depends on the temperature T, the time step Δt, and the cell volume ΔV.

For the sake of comparability the same simulation parameters as for the simulations without temperature dependence were employed. The more interesting smaller free layer sizes 10 nm × 40 nm × 3 nm and 20 nm × 80 nm × 3 nm were studied. The parameter s was set to 0., 0.01, 0.02, 0.05, 0.1, 0.2, 0.5, 0.75, and 1.0 for one SET input combination, two HOLD input combinations, and simulations without any signal for stability testing. The pulse window length was extended from 20 ns to 40 ns to check the assumption that the reduction in switching time at high disturbance strength (cf. Fig. 5) is caused by the cut of the switching time distribution [24]. The thermal field $\vec{H}_{\mathrm{th}}$ was present for all simulations.

4. Results

4.1. Static disturbance without thermal excitations

For the first set of simulations it was at first checked how the free layer behaves without any current pulse applied. The free layer's magnetization was set parallel to the z-axis plus a small initial deviation from its out-of-plane anisotropy position and then allowed to evolve in time without external forces. Thus, the influence of the random fluctuations on the free layer's ability to hold information in general was tested. The free layer keeps perfectly its initial orientation until s reaches about 50% of the saturation magnetization. At $s = 0.5$ the fluctuations become so strong that more and more of the test structures started to flip (Fig. 4). The close switching times for 20 nm and 30 nm layers, shown in Fig. 4, stem from the non-linear dependence of the thermal barrier on the shape anisotropy of the free layer [21].

Fig. 5 shows the average switching time and the corresponding error bars show $\pm\sigma$ for the SET operation (two synchronous identical pulses) as a function of the free layer's size and relative strength parameter. One can see that for up to $s = 0.2$ there is no

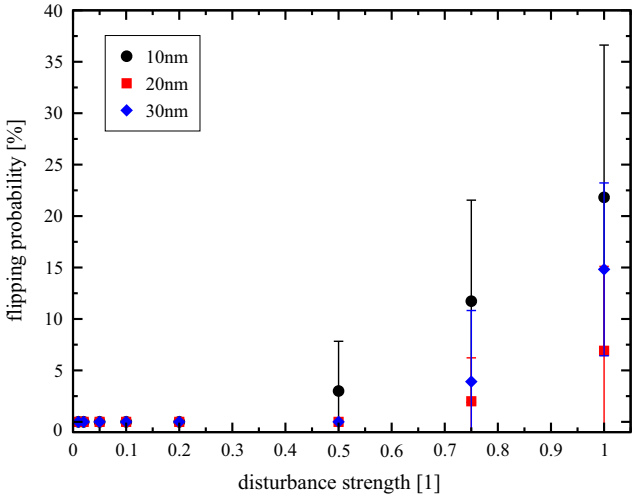

Fig. 4. Simulations to check at which level of added randomization the free layer will flip its orientation without external force.

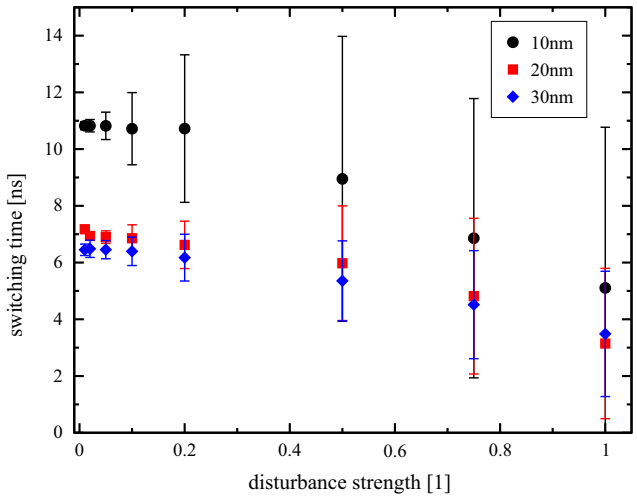

Fig. 5. Switching time as a function of free layer size and disturbance strength.

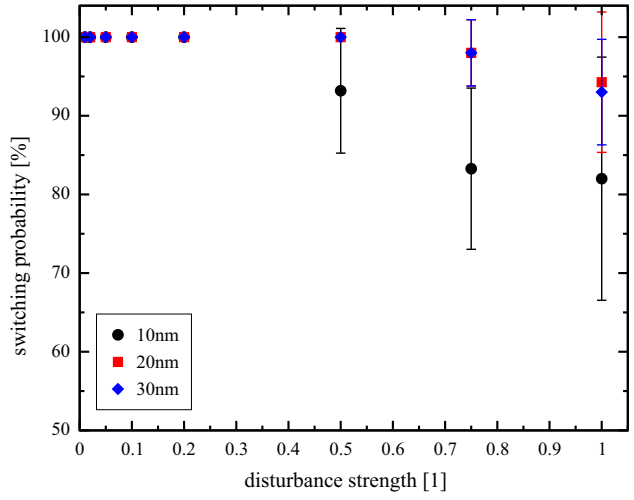

Fig. 6. Switching probabilities for Fig. 5. For 20 nm and 30 nm the structure switches perfectly until disturbed with 50% of M_S and for 10 nm until 20% of M_S.

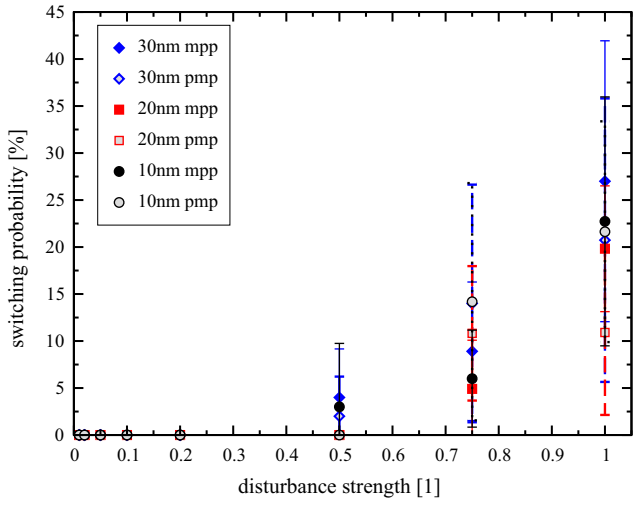

Fig. 7. Switching probabilities as a function of disturbance strength and free layer size. The three letters following the layer width denote the applied input polarities and the initial magnetization orientation of the free layer ($- = m$, $+ = p \rightarrow A, B,\ Q_0$).

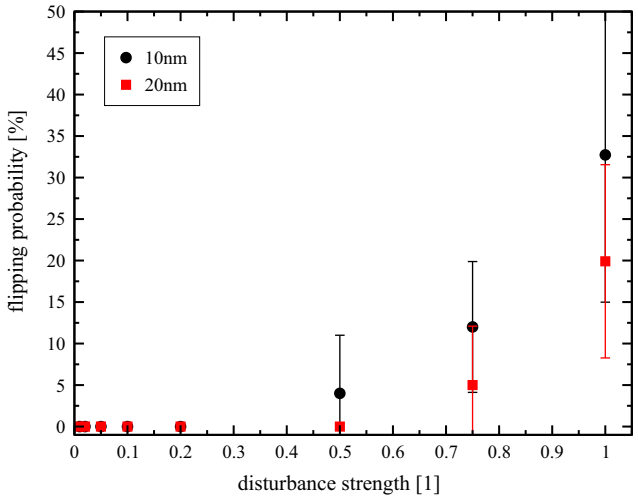

Fig. 8. Simulations to test at which level of added randomization the free layer will flip its orientation without external force, due to the thermal field $\vec{H}_{th}$.

significant change in the switching times, but as expected the distribution of switching times broadens with increasing relative strength parameter s. Actually, it starts to broaden so much above $s = 0.2$ that the pulse window is not sufficiently long anymore to switch all layers in time. Additionally, as illustrated in Fig. 4, the layer's stability starts to decrease and the downwards position becomes more favorable. The reason for the shift towards shorter switching times is elucidated in Section 4.2. The same effect is also reflected in Fig. 6, where at $s = 0.5$ the switching probability for 10 nm layer width starts to drop below 100%, which is the case for 20 nm and 30 nm layer width at $s = 0.75$.

In contrast to the SET operation, the HOLD operation demands that the free layer magnetization does not change, when the two opposing pulses are applied. This again holds true for s between 0.2 and 0.5 (see Fig. 7).

4.2. Static disturbance with thermal excitations

For the second set of simulations thermal excitations were added to study their influence on the device behavior and possible interactions with the static normally distributed random field. If one now looks at the free layer's capability to keep its current magnetization orientation as a function of disturbance strength (cf. Fig. 8), one can observe that like in Fig. 4 the device keeps its orientation (0% switching probability) until $s = 0.2$ for 10 nm and $s = 0.5$ for 20 nm. This is consistent with the standard deviation of the thermal field $\vec{H}_{th}$ of ≈ 2.3 kA/m at 300 K and the comparatively large magnetization saturation $M_S = 4 \times 10^5$ A/m and anisotropy field $\vec{H}_{K_1} \approx 2 \times 10^5$ A/m. However, with increasing disturbance strength the thermal fluctuations add to the flipping probability ($s = 0.5$ $3\% \rightarrow 4\%$, $s = 1.0$ $22\% \rightarrow 33\%$ for 10 nm and $s = 0.75$ $2\% \rightarrow 5\%$, $s = 1.0$ $7\% \rightarrow 20\%$ for 20 nm). Fig. 9 shows the switching time for the SET operation as a function of disturbance strength and layer size including thermal fluctuations. At $s = 0$ the static disturbance distribution was switched off to get pure thermal excitation switching times. Due to the comparatively small thermal field $\vec{H}_{th}$ for low disturbance strength the differences in switching time and standard deviations are modest. Again with increasing disturbance strength the two contributions start to add up and lead to a slightly increased switching time $\approx 1 - 1.5$ ns and standard deviation $\approx 1 - 2$ ns for 10 nm and < 0.8 ns and < 0.5 ns

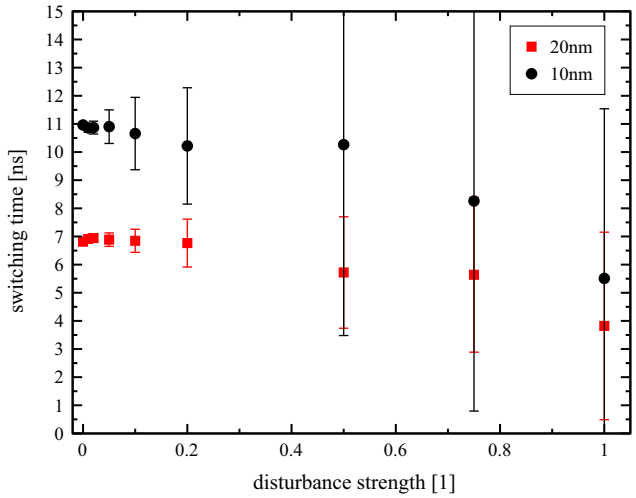

Fig. 9. Switching time for the SET operation as a function of layer size and disturbance strength including the thermal field $\vec{H}_{th}$.

for 20 ns, respectively. The corresponding switching probabilities for the SET operation are shown in Fig. 10. While the switching probability degrades for a layer size of 10 nm, when thermal excitations are considered, the opposite seems to happen for a layer size of 20 nm. A thorough examination of the respective simulation samples revealed that at elevated disorder levels a non-neglectable percentage ($s = 0.75 \rightarrow 4\%$ and $s = 1.0 \rightarrow 13\%$) of the samples data show large and stable precessional motions, which where accounted for successful switching by the automated analysis and thus led to the shift in the results. Figs. 11 and 12 illustrate the switching time probabilities as a function of switching time and disturbance strength for the SET operation. Both plots exhibit time steps of 0.5 ns and a total time window of 40 ns. While the switching time distribution is very narrow for small disturbance strength, above $s = 0.1$ it starts to broaden. Due to the increasing disorder, when s is increased, the effective anisotropy of the free layer becomes smaller and the Gaussian distributed statistical variations start to dominate the switching behavior. The decreasing effective anisotropy leads to a reduced switching barrier and thus to reduced switching times (see Figs. 5 and 9). By comparing Figs. 11 and 12 one also observes a stronger spread in switching probabilities for the smaller free layer. This can be explained by

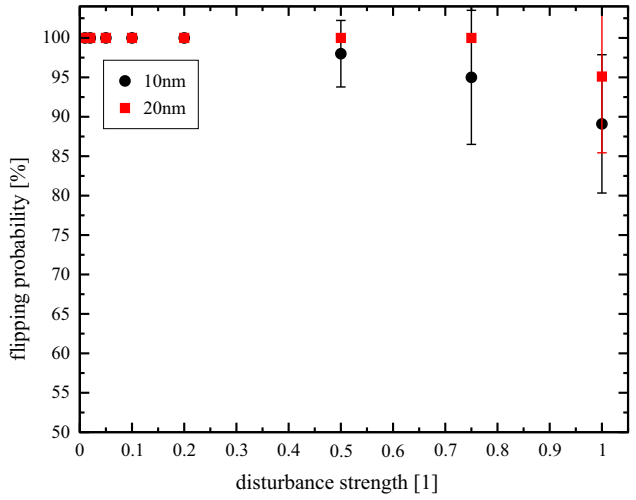

Fig. 10. Switching probability for the SET operation as a function of layer size and disturbance strength including the thermal field $\vec{H}_{th}$.

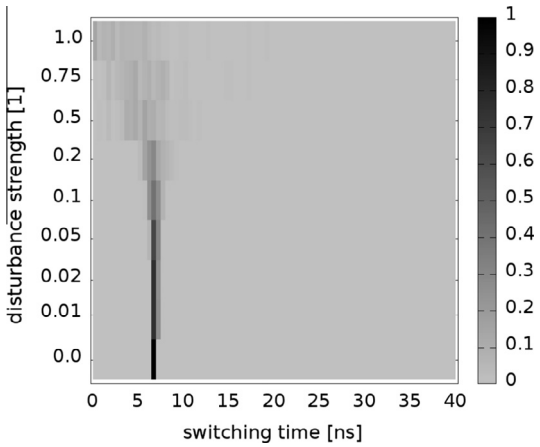

Fig. 11. Normalized switching time distributions for 20 nm. The switching probability as a function of time and disturbance strength is encoded as color (from 0% → grey to 100% → black).

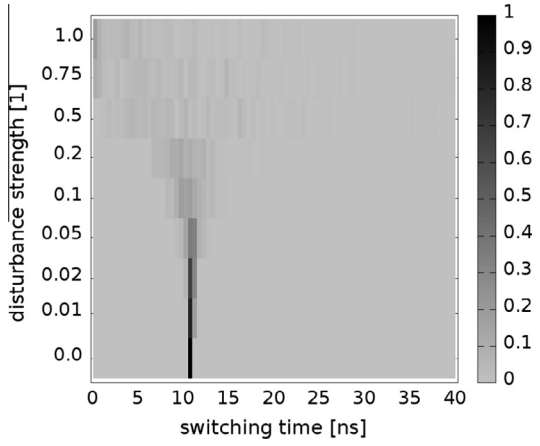

Fig. 12. Normalized switching time distributions for 10 nm. The switching probability as a function of time and disturbance strength is encoded as color (from 0% → grey to 100% → black).

the smaller total magnetic moment in the layer with 10 nm width compared to the layer with 20 nm width. Fig. 13 depicts the switching probabilities for the HOLD operation as a function of free layer size and disturbance strength. The overall switching probabilities arereduced in comparison to Fig. 6. This means that the thermal field acts as a damping force and actually improves the device stability. However, for some points the switching probability actually increases, e.g. $10\,\text{nm}, \text{pmp}, s = 1.11\% \rightarrow 20\%$ and $20\,\text{nm}, \text{mpp}, s = 0.755\% \rightarrow 10\%$. It is known that for the HOLD operation stable precessional motions are excitable [25]. This precessional motions cause a shift in the switching probabilities like in the SET operation.

5. Discussion

The influence of the thermal field on the free layers capability to keep its initial magnetization orientation is marginal. Only at elevated disturbance strength and when the effective anisotropy is weak the magnetization flips under thermal excitations. Therefore, for low disturbance strength it is sufficient to neglect thermal fluctuations, which allows a variable time stepping scheme to speed up the simulation. If on the other hand it is required to study elevated disturbance strengths or to include strong thermal excitations (4) must be considered at the cost of a fixed time step and increased computation time.

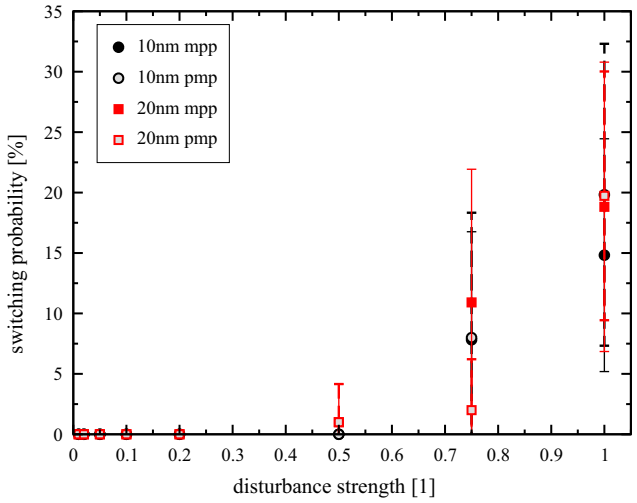

Fig. 13. Switching probabilities as a function of disturbance strength and free layer size. The three letters following the layer width denote the applied input polarities and the initial magnetization orientation of the free layer (A, B, Q_0).

The reduction in switching time for increasing disorder shown in Fig. 5 is not only due to the pulse window limitation to 20 ns as assumed previously [24]. This becomes evident by looking at the simulation data for the 40 ns time window (see Figs. 9, 11, and 12). The drop in switching time is still present and the thermal field only adds moderate changes. The switching time probabilities shown in Figs. 11 and 12 indeed demonstrate that a 40 ns window is long enough to cover the full distribution. Additionally, it can be observed that the center (mean) of the distribution shifts towards shorter switching times. Therefore, it is more likely that the static random field reduces the effective anisotropy of the free layer. The reduced effective anisotropy diminishes the switching barrier and thus leads to reduced switching times for increasing disturbance strength s.

Finally, for the HOLD operation, with its two opposing spin transfer torques, the thermal fluctuations damp the precessional motions in the free layer, thus, aiding the device stability.

6. Conclusion

Recapitulatory, it could be shown that the presented flip flop is capable of safely operating under quite high free layer inhomogeneities with thermal fluctuations at 300 K. Two sets of simulations were analyzed and compared. The first set neglects temperature effects and assumes space uncorrelated and fixed in time normal distributions for the free layer inhomogeneities. The second set includes a time step dependent random thermal field.

The chosen approach allows easily to test different distribution types and requires only a minimal software adaption. Nevertheless, a big layer magnetization variance leads to broad switching time distributions which might lead to timing problems, e.g. in the worst case the whole circuit will be slowed down by a single device.

Acknowledgment

This work is supported by the European Research Council through the Grant #247056 MOSILSPIN.

References

[1] International Technology Roadmap for Semiconductors, Chapter PIDS; 2012. <http://www.itrs.net/Links/2012ITRS/Home2012.htm>.

[2] Zhao W, Torres L, Guillemenet Y, Cargnini LV, Lakys Y, Klein J-O, Ravelosona D, Sassatelli G, Chappert C. Design of MRAM based logic circuits and its applications. In: ACM great lakes symposium on VLSI; 2011, p. 431–6. doi:10.1145/1973009.1973104.

[3] Kim N, Austin T, Baauw D, Mudge T, Flautner K, Hu J, et al. Leakage current: moore's law meets static power. Computer 2003;36(12):68–75. http://dx.doi.org/10.1109/MC.2003.1250885.

[4] Nikonov D, Young I. Overview of beyond-CMOS devices and a uniform methodology for their benchmarking. Proc IEEE 2013;101(12):2498–533. http://dx.doi.org/10.1109/JPROC.2013.2252317.

[5] Mahmoudi H, Windbacher T, Sverdlov V, Selberherr S. Reliability-based optimization of spin-transfer torque magnetic tunnel junction implication logic gates. Adv Mater Res 2014;854:89–95. http://dx.doi.org/10.4028/www.scientific.net/AMR.854.89.

[6] Mahmoudi H, Windbacher T, Sverdlov V, Selberherr S. Implication logic gates using spin-transfer-torque-operated magnetic tunnel junctions for intrinsic logic-in-memory. Solid-State Electron 2013;84:191–7. http://dx.doi.org/10.1016/j.sse.2013.02.017.

[7] Everspin Technologies, Jan. 2014. <http://www.everspin.com/spinTorqueMRAM.php>.

[8] Slaughter J, Aggarwal S, Alam S, Andre T, Chia HJ, DeHerrera M, Deshpande S, Houssameddine D, Janesky J, Mancoff FB, Nagel K, Schneider ML, Rizzo ND, Whig R. Properties of CMOS-integrated magnetic tunnel junction arrays for spin-torque magnetoresistive random access memory. In: Abstracts of the 58th annual conference on magnetism and magnetic materials, symposium on materials advances of spin-torque switched memory devices for silicon integration, 2013, pp. BA–01.

[9] Worledge D, Brown SL, Chen W, Harms J, Hu G, Kilaru R, Kula W, Lauer G, Liu LQ, Nowak J, Parkin S, Pushp A, Murthy S, Robertazzi RP, Sandhu G, Sun J. Materials advances in perpendicularly magnetized *mgo*-tunnel junctions for STT-MRAM. In: Abstracts of the 58th annual conference on magnetism and magnetic materials, symposium on materials advances of spin-torque switched memory devices for silicon integration; 2013, p. BA–02.

[10] Thomas L, Jan G, Zhu J, Liu H, Lee Y, Le S, Tong R, Pi K, Wang Y, Zhong T, Torng T, Wang P. Magnetization dynamics in perpendicular STT-MRAM cells with high spin-torque efficiency and thermal stability. In: Abstracts of the 58th annual conference on magnetism and magnetic materials, symposium on materials advances of spin-torque switched memory devices for silicon integration; 2013, p. BA–03.

[11] Windbacher T, Mahmoudi H, Sverdlov V, Selberherr S. Rigorous simulation study of a novel non-volatile magnetic flip flop. In: Proc. intl. conf. on simulation of semiconductor processes and devices (SISPAD); 2013, p. 368–71.

[12] Windbacher T, Mahmoudi H, Sverdlov V, Selberherr S. Spin torque magnetic integrated circuit, EP13161375, March 2013. <www.iue.tuwien.ac.at/pdf/ib_2013/PT2014_Windbacher_1.pdf>.

[13] Hertel R. Handbook of magnetism and advanced magnetic materials. John Wiley & Sons, Ltd; 2007. Ch. Guided Spin Waves. doi:http://dx.doi.org/10.1002/9780470022184.hmm202.

[14] Tietze U, Schenk C. Electronic circuits – handbook for design and applications, 2nd ed., Vol. 12. Springer; 2008.

[15] Donahue M, Porter D. OOMMF User's Guide, Interagency Report NISTIR 6376, National Institute of Standards and Technology, Gaithersburg, MD, version 1.0. September 1999.

[16] Gilbert T. A lagrangian formulation of the gyromagnetic equation of the magnetization field. Phys Rev 1955;100:1243.

[17] Kronmüller H. Handbook of magnetism and advanced magnetic materials. John Wiley & Sons, Ltd; 2007. Ch. General Micromagnetic Theory. doi:http://dx.doi.org/10.1002/9780470022184.hmm202.

[18] Khvalkovskiy AV, Zvezdin KA, Gorbunov YV, Cros V, Grollier J, Fert A, et al. High domain wall velocities due to spin currents perpendicular to the plane. Phys Rev Lett 2009;102:067206. http://dx.doi.org/10.1103/PhysRevLett.102.067206.

[19] Xiao J, Zangwill A, Stiles MD. Boltzmann test of slonczewski's theory of spin-transfer torque. Phys Rev B 2004;70:172405. http://dx.doi.org/10.1103/PhysRevB.70.172405.

[20] Miltat JE, Donahue MJ. Handbook of magnetism and advanced magnetic materials. John Wiley & Sons, Ltd; 2007. Ch. Numerical Micromagnetics: Finite Difference Methods. doi:http://dx.doi.org/10.1002/9780470022184.hmm202.

[21] Windbacher T, Mahmoudi H, Sverdlov V, Selberherr S. Influence of device geometry on the non-volatile magnetic flip flop characteristics. In: Proc. intl. conf. on simulation of semiconductor processes and devices (SISPAD); 2014, to be published.

[22] Brown WF. Thermal fluctuations of a single-domain particle. Phys Rev 1963;130:1677–86. http://dx.doi.org/10.1103/PhysRev.130.1677.

[23] Ito K, Devolder T, Chappert C, Carey MJ, Katine JA. Probabilistic behavior in subnanosecond spin transfer torque switching. J Appl Phys 2006;99(8). http://dx.doi.org/10.1063/1.2176869.

[24] Windbacher T, Mahmoudi H, Sverdlov V, Selberherr S, Influence of magnetization variations in the free layer on a non-volatile magnetic flip flop. In: Proc. intl. conf. on ultimate integration on silicon (ULIS); 2014, p. 9–12. doi:10.1109/ULIS.2014.6813893.

[25] Windbacher T, Makarov A, Mahmoudi H, Sverdlov V, Selberherr S. Novel bias-field-free spin transfer oscillator. J Appl Phys 2014;115(17):1–3. http://dx.doi.org/10.1063/1.4862936.